Analysis of the impact of a sharp indenter

E.W. Andrews [a], A.E. Giannakopoulos [a], E. Plisson [b], S. Suresh [a,*]

[a] *Department of Materials Science and Engineering, Massachusetts Institute of Technology, RM 8-309, 77 Massachusetts Avenue, Cambridge, MA 02139, USA*
[b] *Ecole Polytechnique, 91128 Palaiseau Cedex, France*

Abstract

The present work investigates the impact of a sharp indenter at low impact velocities. A one-dimensional model is developed by assuming that the variation of indentation load as a function of depth under dynamic conditions has the same parabolic form (Kick's Law) as under static conditions. The motion of the indenter as it indents and rebounds from the target is described. Predictions are made of the peak indentation depth, residual indentation depth, contact time, and rebound velocity as functions of the impact velocity, indenter mass and target properties. Finite element simulations were carried out to assess the validity of the model for elastoplastic materials. For rate-independent materials agreement with the model was good provided the impact velocity did not exceed certain critical values. For rate-dependent materials the relationship between load and depth in the impact problem is no longer parabolic and the model predictions cannot be applied to this case. The rate-dependent case can be solved by incorporating the relationship between the motion of the indenter and the dynamic flow properties of the material into the equation of motion for the indenter. © 2001 Elsevier Science Ltd. All rights reserved.

Keywords: Indentation; Impact; Dynamic plasticity

1. Introduction

We consider here the impact of a sharp indenter. Indentation problems are difficult to analyze: the problem is generally three-dimensional, a complicated contact problem must be solved at the interface of the indenter and the target, and material nonlinearities due to plasticity, friction, phase transformations and microcracking are often involved. For the case of an impact problem, target inertia and rate-dependent material behavior add to the complexity of the problem. The impact of a sharp indenter is a problem of considerable technological interest, both as a means of assessing dynamic material behavior and for evaluating the damage caused by the impact of small, sharp particles on various types of structures. Impacts of this kind on aircraft bodies and engine components, termed foreign object damage (FOD), is a significant concern to airframe and aircraft engine manufacturers.

* Corresponding author. Tel.: +1-617-253-3320; fax: +1-617-253-0868.
E-mail address: ssuresh@mit.edu (S. Suresh).

Indentation tests provide a nondestructive method for extracting several basic material properties, at various size scales. Nearly all standard instrumented indentation tests are carried out under quasi-static conditions. Results have been reported for dynamic indentation tests using sharp (Graham, 1973; Marshall et al., 1983; Koeppel and Subhash, 1999) and spherical indenters (Tirupataiah and Sundararajan, 1991). A dynamic indentation test offers the possibility of determining the dynamic hardness and rate-dependent response of the material.

In this paper, we analyze the impact of a sharp indenter in the context of dynamic elastoplasticity. In Sections 2 and 3 we analyze theoretically and computationally the case of rate-independent response of the target. In Section 4, we analyze computationally the case of rate-dependent response of the target and provide a general methodology to relate the impact response with the rate-dependent plastic properties of the target.

2. Analytical one-dimensional model

The indenter is assumed to be sharp, such as a pyramid or circular cone indenter. The indenter is assumed to be rigid. It has a mass m and contacts the target at an initial velocity V_0 normal to the surface. The target is assumed to be a rate-independent, elastoplastic, homogeneous, isotropic body whose dimensions are large compared to the contact diameter. The contact is assumed to be frictionless. Prior to the impact, the target is stress-free and at rest.

For sharp indentation under quasi-static conditions, if P is the force exerted by the indenter on the target and h is the depth of indentation, the P–h curve follows a parabolic relation during loading, i.e. $P = Ch^2$, known as Kick's law. The unloading curve is assumed to be linear. The slope of the unloading curve reflects the elastic properties of the indenter and the target, as well as the area of contact at the instant of unloading. Note that as the load approaches zero, typically the unloading curve becomes nonlinear. However, a linear unloading curve is employed in this analysis. We define a new constant C_e in terms of the unloading slope dP/dh and the peak indentation depth h_{max} as $dP/dh = C_e h_{max}$. The constant C_e has the same units as C. By asserting that the contact area corresponding to elastic response at the maximum load should be less than or equal to the actual contact area it can be shown that the slope of the unloading curve must be greater than or equal to the instantaneous slope of the loading curve at the point of unloading. This requires that C/C_e must be less than or equal to 0.5. Fig. 1 shows the loading and unloading curves for various allowable
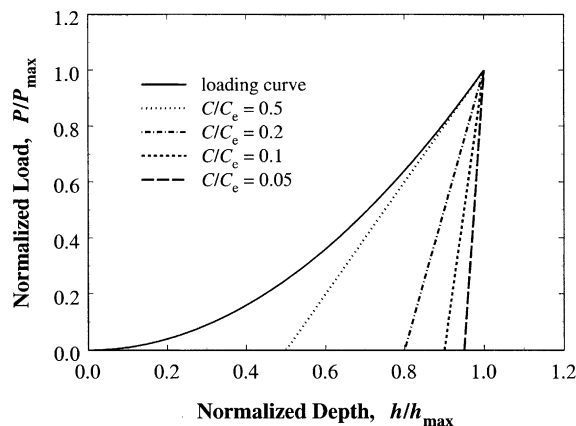

Fig. 1. Force–depth curves showing allowable values of the unloading slope.

values of the dimensionless parameter C/C_e. Expressions for C and the unloading slope for various sharp indenter geometries under static conditions are available (e.g. Giannakopoulos and Suresh, 1999).

During the impact, the motion $h(t)$ of the indenter is governed by Newton's second law:

$$m\ddot{h} + P = 0. \tag{1}$$

The velocity and acceleration of the indenter will be denoted by $\dot{h}$ and $\ddot{h}$, respectively. Time $t = 0$ is taken to be the instant when the indenter touches the target. The motion of the indenter has three phases: an indentation phase, a rebound phase and a free-flight phase. During the indentation phase, the velocity of the indenter decreases as the initial kinetic energy is converted to energy associated with deformation of the target. Part of the initial energy is stored as elastic energy which is recovered in the rebound phase, while the rest is dissipated as plastic work.

To analyze the impact problem it is assumed that the shape of the P–h curve is unchanged under dynamic conditions. If the impact velocity is high enough the kinetic energy of the target becomes significant. Furthermore, adiabatic heating and thermal softening, localization of the deformation, phase transformations or even melting of the material can occur under dynamic conditions. Under these conditions, the dynamic P–h curve will not follow the quasi-static curve and this analysis will not be valid. Assuming that the quasi-static curve is followed during the indentation phase P increases with h as $P = Ch^2$ so we have that

$$m\ddot{h} + Ch^2 = 0; \quad t \geqslant 0 \tag{2}$$

with initial conditions $h = 0$ and $\dot{h} = V_0$ at $t = 0$. Integration of Eq. (2) leads to the energy balance expression:

$$\tfrac{1}{2}m\dot{h}^2 - \tfrac{1}{2}mV_0^2 = -\tfrac{1}{3}Ch^3. \tag{3}$$

The maximum penetration depth $h_{\max}$ can be determined from Eq. (3) by setting $\dot{h} = 0$ and solving for h:

$$h_{\max} = \left(\frac{3mV_0^2}{2C}\right)^{1/3}. \tag{4}$$

Eq. (3) can be integrated with respect to time to obtain the duration of the penetration phase t_1, i.e. the time taken to reach $h_{\max}$:

$$t_1 = \int_0^{h_{\max}} \left(V_0^2 - \frac{2}{3}\frac{Ch^3}{m}\right)^{-1/2} \mathrm{d}h = \left(\frac{3m}{2CV_0}\right)^{1/3}\left[\frac{1}{3}\beta\left(\frac{1}{3},\frac{1}{2}\right)\right] = 1.402\left(\frac{3m}{2CV_0}\right)^{1/3}, \tag{5}$$

where β is the beta function (Euler's integral of the first kind) defined as

$$\beta(x,y) = \int_0^1 t^{x-1}(1-t)^{y-1}\,\mathrm{d}t. \tag{6}$$

More generally, if $t(h)$ is the time taken by the indenter to penetrate to a depth h of the target, a similar calculation gives:

$$t(h) = \int_0^h \left(V_0^2 - \frac{2}{3}\frac{Cu^3}{m}\right)^{-1/2} \mathrm{d}u = \left(\frac{3m}{2CV_0}\right)^{1/3}\int_0^{h/h_{\max}} \frac{\mathrm{d}x}{\sqrt{1-x^3}}. \tag{7}$$

During the rebound phase, the load follows the linear unloading curve shown in Fig. 1. During unloading the load may be expressed as $P = C_e h_{\max} h + (C - C_e)h_{\max}^2$. This expression comes from the definition of the unloading slope, and using the condition that the load P is equal to $Ch_{\max}^2$ at $h = h_{\max}$. The motion of the indenter is governed by

$$m\ddot{h} + C_e h_{\max} h + (C - C_e)h_{\max}^2 = 0, \quad t \geqslant t_1 \tag{8}$$

with initial conditions $h = h_{\max}$ and $\dot{h} = 0$ at $t = t_1$. The solution of this differential equation is

$$h(t) = h_{max}(1 - \bar{C} + \bar{C}\cos(\omega t - \omega t_1)), \tag{9}$$

where $\omega = (C_e h_{\max}/m)^{1/2}$ and $\bar{C} = C/C_e$. The indenter accelerates away from the target until the force P decreases to 0. From the expression for the unloading curve the depth h_2 when $P = 0$ can be found to be

$$h_2 = h_{\max}(1 - \bar{C}). \tag{10}$$

The depth h_2 represents the final or residual indentation depth; the difference between $h_{\max}$ and h_2 corresponds to the elastic recovery of the target. By setting $h(t) = h_2$ in Eq. (9) the time t_2 when $P = 0$ can be found to be

$$t_2 = t_1 + \frac{\pi}{2}\left(\frac{m}{C_e h_{\max}}\right)^{1/2}. \tag{11}$$

During the final (free-flight) phase the indenter and the target are no longer in contact. No forces act on the indenter; it moves away from the target at constant velocity. In this phase the velocity, $\dot{h}$, is equal to its value at $t = t_2$. This rebound velocity can be determined by differentiation of Eq. (9) and setting $t = t_2$:

$$V_{\text{rebound}} = -V_0\left(\frac{3\bar{C}}{2}\right)^{1/2}. \tag{12}$$

The position during the free-flight phase is given as

$$h(t) = h_2 - (t - t_2)\left(\frac{3\bar{C}V_0^2}{2}\right)^{1/2}. \tag{13}$$

The absolute value of the ratio of the rebound velocity to the impact velocity, the coefficient of restitution e, is evaluated using Eq. (12) to be

$$e = \left|\frac{V_{\text{rebound}}}{V_0}\right| = \left(\frac{3\bar{C}}{2}\right)^{1/2}. \tag{14}$$

The coefficient of restitution is independent of the impact velocity. In terms of a normalized time $\bar{t} = t/t_1$ and a normalized indentation depth $\bar{h} = h/h_{\max}$, the motion of the indenter may be written as

$$\bar{t}(\bar{h}) = 0.713\int_0^{\bar{h}}\frac{\mathrm{d}x}{\sqrt{1 - x^3}} = 0.713\bar{h}F(1/3, 1/2; 4/3; \bar{h}^3), \quad 0 \leqslant t \leqslant t_1 \tag{15}$$

$$\bar{h}(\bar{t}) = \bar{C}\left(\cos\left(\frac{\bar{t} - 1}{0.582\,\bar{C}^{1/2}}\right) - 1\right) + 1, \quad t_1 < t \leqslant t_2 \tag{16}$$

$$\bar{h}(\bar{t}) = \bar{h}_2 - (\bar{t} - \bar{t}_2)(2.948\,\bar{C})^{1/2}, \quad t > t_2. \tag{17}$$

In the above expressions, F is the hypergeometric function, $\bar{h}_2 = 1 - \bar{C}$, and $\bar{t}_2 = 1 + 0.915(\bar{C})^{1/2}$. The complete motion of the indenter is shown in Fig. 2 which plots the function $\bar{h}(\bar{t})$ for various values of the dimensionless ratio C/C_e. Marshall et al. (1983) considered the impact of a sharp indenter and provided expressions for the peak depth $h_{\max}$ and loading time t_1 analogous to Eqs. (4) and (5). The present study extends their analysis by considering the rebound phase, and providing expressions for the complete motion of the indenter. The rebound phase can be important if elastic deformation of the target is significant (e.g. brittle materials).
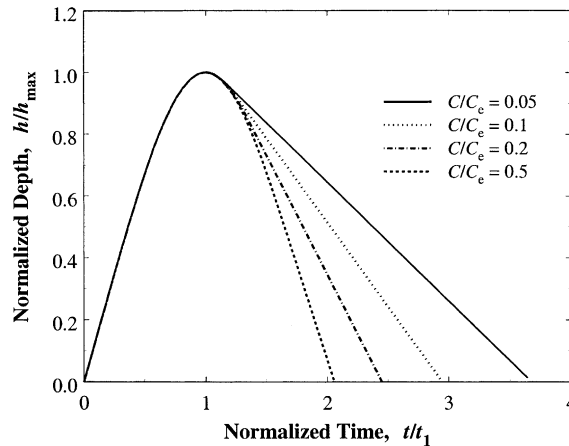
Fig. 2. Analytical prediction of normalized indentation depth vs. normalized time for various values of C/C_e.

3. Finite element simulations for rate-independent materials

In this section the results of a finite element study are presented. The objective is to assess the range of validity of the analytical results presented in Section 2. The commercial finite element package ABAQUS/ Explicit (HKS, Pawtucket, RI) was used to simulate the impact. The mesh used is shown in Fig. 3(a). A typical deformed mesh at the peak depth of indentation is shown in Fig. 3(b). The simulation uses infinite elements away from the contact area to simulate a semi-infinite region. The mesh has a total of 19,200 axisymmetric, 4-noded, reduced integration, continuum elements, and 160 infinite elements at the boundary. Although the analytical results in Section 2 apply for any sharp indenter, in these simulations the indenter is considered to be a cone with a 70.3° included half angle. This gives approximately the same ratio of indentation depth to contact area as the common Vickers and Berkovich indenters. At the peak depth of indentation approximately 14–18 elements spanned the contact radius. Large deformation analysis and the adaptive meshing option were employed. The indenter was represented as a rigid surface with an associated mass element. To study the role of indenter mass two different values were used: $m = 10$ mg and 10 g. The impact velocity V_0 varied from 0.5 to 1800 m/s. The simulations were isothermal; heating of the material and the associated thermal softening were not included.

To consider a variety of materials, the stress–strain response of the target was represented by four different elastoplastic materials: 6061 Aluminum (Giannakopoulos et al., 1994), annealed commercial brass (ASM, 1979), mild steel and 4340 steel (ASM, 1987). Classical Mises elastoplastic behavior was assumed, i.e. isotropic linear hypoelasticity and incremental plastic strains calculated using an associated Mises flow rule. Fig. 4 shows the uniaxial tensile true stress–logarithmic plastic strain curves for these materials. These curves are from quasi-static tests. In some cases the uniaxial data did not extend out to the large strains necessary to carry out the indentation simulations; in these cases the data were extended assuming constant strain hardening. Values of C and C_e for each material were determined from quasi-static simulations and are reported in Table 1.

In order to compare the finite element analysis (FEA) results with the analytical results, we will first compare with the predicted maximum indentation depth h_{max}. The expression for h_{max} in Eq. (4) can be rewritten as follows:

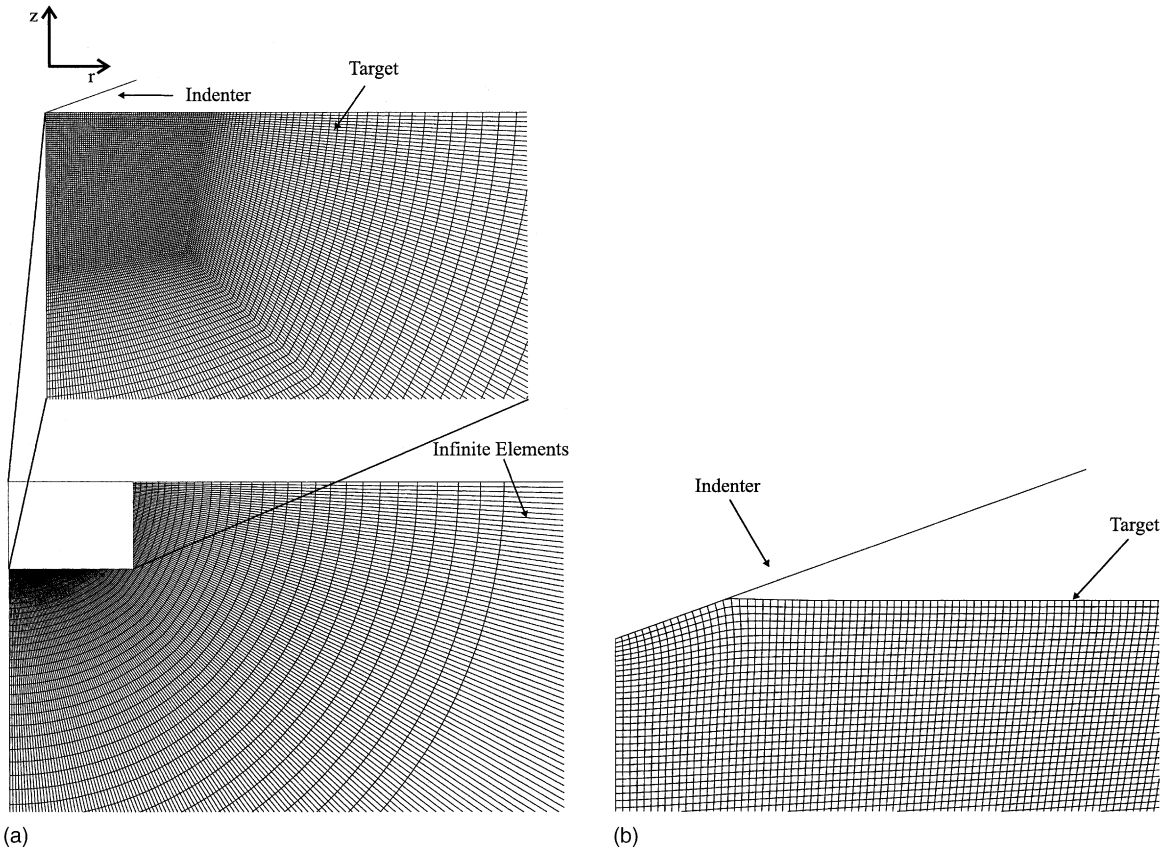$$h_{max} = h_t \left(\frac{V_0}{V_t} \right)^{2/3}.$$

(18)

Fig. 3. (a) Finite element mesh used for dynamic indentation simulations. (b) Typical deformed mesh at peak indentation depth.
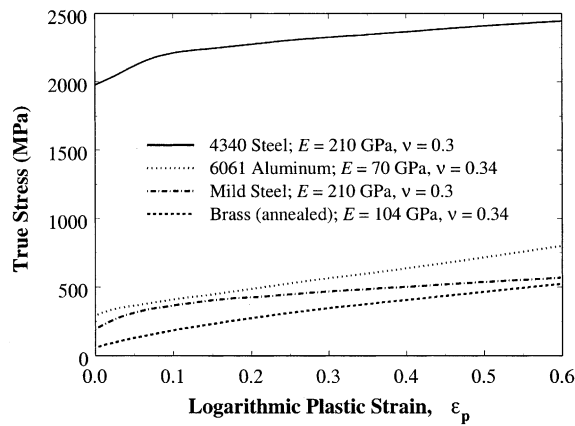

Fig. 4. True stress–logarithmic plastic strain curves for the materials considered in the finite element simulations.

Table 1
Indentation characteristics of the different alloys considered in this study

	Al 6061	Mild steel	4340 steel	Brass
C (GPa)	30.07	28.32	139.20	12.50
C_e (GPa)	516.4	1564.4	1334.6	701.7
C/C_e	0.059	0.018	0.104	0.018
ρ_{target} (g/cm^3)	2.7	7.9	7.9	8.5
V_t (m/s)	3337	1905	4224	1220

The quantities h_t and V_t are defined as

$$h_t = \left(\frac{3m}{2\rho_{target}} \right)^{1/3}, \tag{19}$$

$$V_t = \left(\frac{C}{\rho_{target}} \right)^{1/2}, \tag{20}$$

where ρ_{target} is the mass density of the target material. The velocity V_t is a characteristic velocity for the dynamic sharp indentation problem. As V_0 approaches V_t the kinetic energy absorbed by the target becomes significant and results in discrepancies between the simulations and the analytical results. The values of V_t are reported in Table 1. The peak depth (FEA results) as a function of impact velocity is shown in Fig. 5. Eq. (18) suggests that if the normalized depth h_{max}/h_t, is plotted versus the normalized impact velocity V_0/V_t, the results for the different materials and indenter kinetic energies should fall on the same curve. Fig. 6 shows this plot. It can be seen that up to a velocity of approximately $0.1V_t$ good agreement holds between the theory and the FEA results, above that velocity the depths seen in the simulations are less than those predicted by the theory.

An additional way to assess the range of validity of the analysis is to examine the coefficient of restitution e. Recall from Eq. (14) that e should be independent of the impact velocity and depends only on the ratio C/C_e. Fig. 7 shows e (FEA results) plotted as a function of impact velocity. Fig. 8 plots the normalized coefficient of restitution (FEA result divided by theoretical prediction) vs. the normalized impact velocity (V_0/V_t). It can be seen that for all four materials the FEA results deviate from the analytical prediction
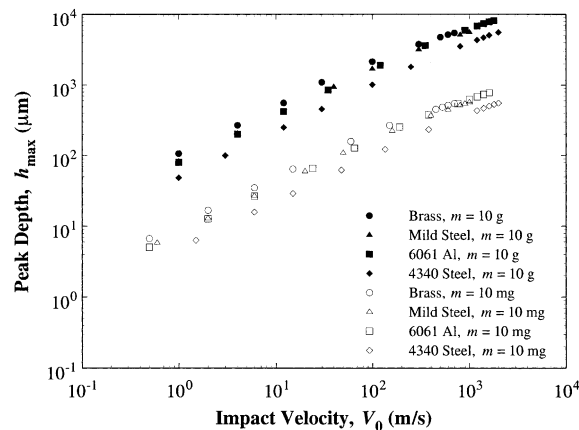

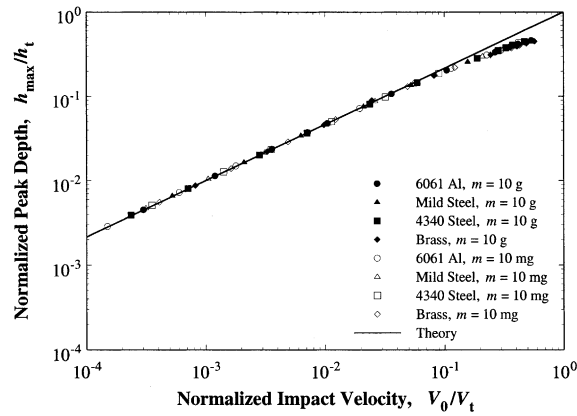Fig. 5. Peak depth vs. impact velocity (FEA results).

Fig. 6. Normalized peak depth vs. normalized impact velocity, along with the analytical result, Eq. (4).
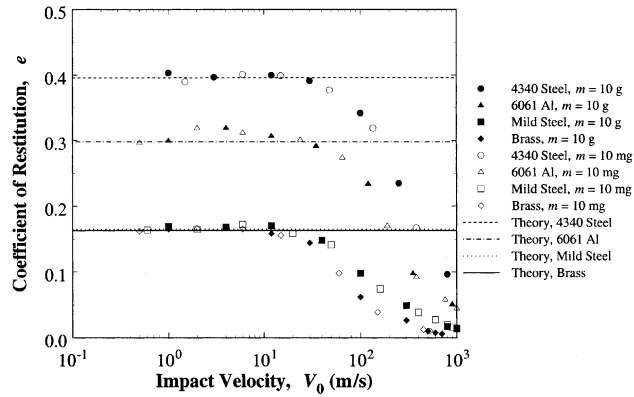

Fig. 7. Coefficient of restitution vs. impact velocity (FEA results). The analytical result, Eq. (14), is also shown.
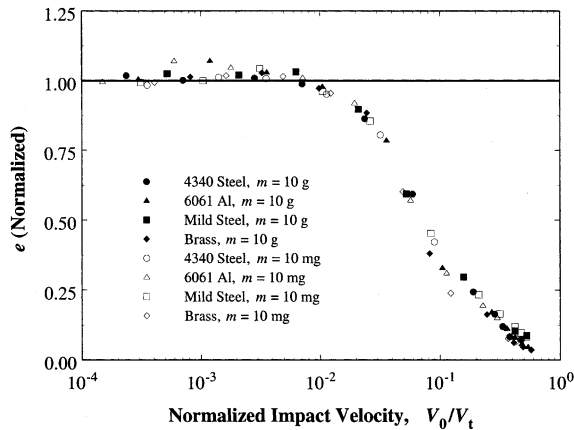

Fig. 8. Normalized coefficient of restitution vs. normalized impact velocity.

when the impact velocity exceeds approximately $0.01V_t$. Below this velocity, the coefficient of restitution is approximately constant and in reasonable agreement with the theory.

As a final means of assessing the range of validity of the analysis, we compare the contact time in the finite element simulations with the theoretical prediction, Eq. (11). The contact time t_2 can be expressed as

$$t_2 = t_t \left(\frac{V_0}{V_t} \right)^{-1/3}, \tag{21}$$

where we have introduced the quantity t_t defined as

$$t_t = \left(\frac{m^2 \rho_{\text{target}}}{C^3} \right)^{1/6} [1.605 + 1.468(\bar{C})^{1/2}]. \tag{22}$$

Fig. 9 shows the contact time t_2 (FEA results) plotted as a function of impact velocity. Eq. (21) suggests that if a normalized contact time, defined as t_2/t_t, is plotted versus the normalized impact velocity, V_0/V_t, the results for the different materials and indenter kinetic energies should fall on the same curve. Fig. 10 plots
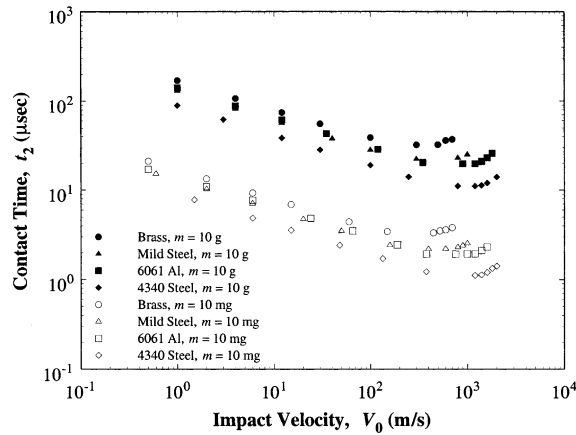

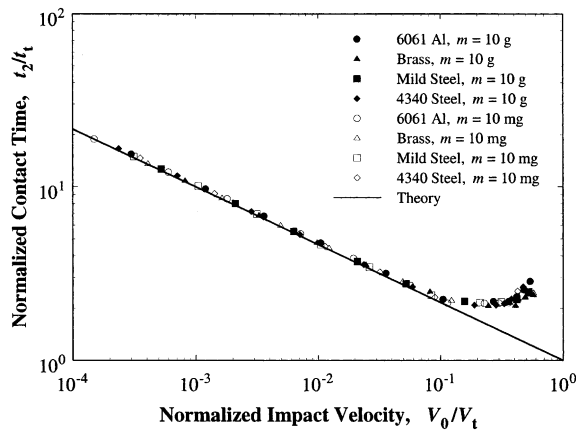Fig. 9. Contact time vs. impact velocity (FEA results).

Fig. 10. Normalized contact time vs. normalized impact velocity, along with the analytical result, Eq. (11).

these results; it can be seen that good agreement is obtained up to impact velocities of $\approx 0.1 V_t$, above that value the contact time observed in the simulations does not continue to decrease as predicted by the theory and instead begins to increase slightly with increasing impact velocity.

The finite element simulations demonstrate the existence of a characteristic velocity V_t which defines the range of validity of the analytical results. As the impact velocity approaches the V_t the role of target inertia, neglected in the analytical model, becomes significant and results in discrepancies between the analytical model and the FEA results seen in Figs. 6, 8 and 10. Comparing the analytical results with the finite element simulations, it appears that quantities associated with the loading phase (e.g. peak depth) show good agreement with the analytical results at impact velocities up to $\approx 0.1 V_t$, while quantities associated with the rebound phase (e.g. rebound velocity) show good agreement up to lower velocities, $\approx 0.01 V_t$. The contact time has a contribution from both the loading phase and the rebound phase. The contribution from the loading phase is significantly larger than that from the rebound phase, hence the contact time shows good agreement with the analytical results at impact velocities up to $\approx 0.1 V_t$.

4. Rate-dependent material response

The simulations in the previous section assumed rate-independent material behavior. In this section we consider the influence of rate-dependent plasticity on the impact of a sharp indenter. It is well known that for some materials the yield stress can vary with the imposed strain rate (e.g. Clifton, 2000; Frantz and Duffy, 1972; Huang and Clifton, 1985; Klopp, 1984; Lee et al., 2000; Li, 1982; Nicholas, 1980; Senseny et al., 1978). Fig. 11 shows the variation in yield stress with strain rate for a variety of metals, showing the increase in flow stress with strain rate. Some of this data is for dynamic shear tests, and the shear quantities have been converted to equivalent uniaxial values. Fig. 12 shows this same data plotted with the dynamic yield stress normalized by the quasi-static yield stress. One way to include the strain rate effect is the power law form

$$\sigma_y(\epsilon, \dot{\epsilon}) = \sigma_y^0(\epsilon)\left(1 + \left(\frac{\dot{\epsilon}}{\dot{\epsilon}_0}\right)^b\right), \tag{23}$$

where b and $\dot{\epsilon}_0$ are material constants. To assess the role of rate-dependent material behavior on the impact of a sharp indenter, finite element simulations using ABAQUS/Explicit were carried out in which the yield
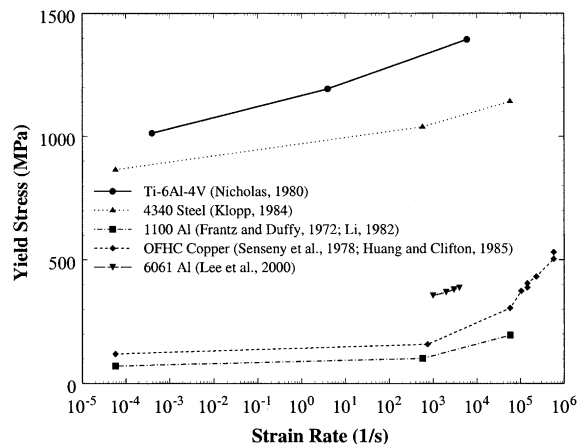

Fig. 11. Yield stress vs. strain rate for a variety of metals showing the increase in yield stress with strain rate.
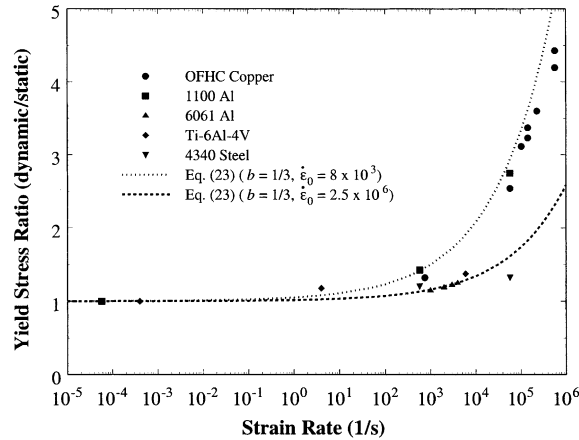
Fig. 12. Yield stress ratio vs. strain rate for the experimental data shown in Fig. 12.

stress varied with strain rate. The mesh used in these simulations was the same as that described in Section 3. A strongly rate sensitive material (with properties corresponding to 1100-O aluminum) and a weakly rate sensitive material (with properties corresponding to 6061 aluminum) were simulated. Values of $b = 1/3$, $\dot{\epsilon}_0 = 8000$ s^{-1} and $b = 1/3$, $\dot{\epsilon}_0 = 250{,}000$ s^{-1} were used for the strongly rate sensitive and weakly rate sensitive materials, respectively. The cases $b = 1/2$ and $\dot{\epsilon}_0 = 8000$ s^{-1} and $b = 1/6$ and $\dot{\epsilon}_0 = 250{,}000$ s^{-1} were also examined. For these materials the variation in flow stress with strain rate is shown in Fig. 12. Material data was defined in such a way that the strain hardening was not rate sensitive.

The effect of rate-dependent material response in dynamic indentation is to increase the resistance to indentation. This effect is illustrated in Fig. 13 which shows the dynamic P–h curve for a simulation in which the rate-dependent response was included for the case of 1100 Aluminum. The indenter mass and impact velocity are 10 mg and 3 m/s, respectively. Even at this low impact velocity, the inclusion of rate-dependent plasticity has the effect of decreasing the peak depth compared to the rate-independent case. The reduction in peak depth, and thus in the final indent size, demonstrates how elevated hardness values are observed under dynamic conditions.
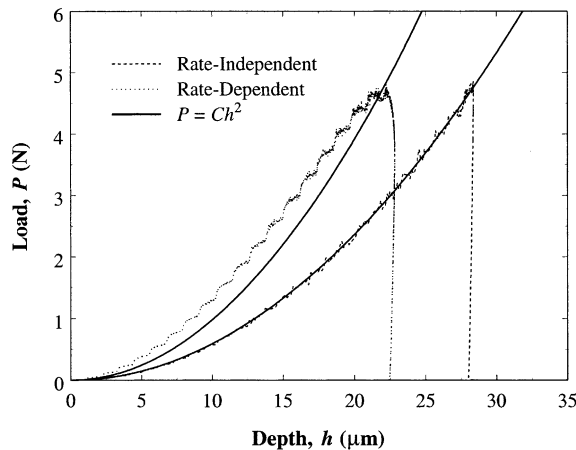

Fig. 13. Load vs. depth in dynamic indentation simulations, rate-dependendent and rate-independent, for 1100 Al, $m = 10$ mg, $V_0 = 3$ m/s.

To assess the validity of Kick's law for the rate-dependent case we attempted to fit curves of the form $P = Ch^2$ to the loading portion of the load–depth curves. A typical result shown in Fig. 13 shows a poor fit. In fact, at the final stages of the loading curve the load becomes constant and then actually decreases slightly. For rate-dependent materials Kick's law is not valid for the impact problem, and therefore the analytical results derived in Section 2 cannot be applied.

Kick's Law is not valid for the rate-dependent case as the loading rates, and thus the material strength, vary during the impact. When the material response is rate-sensitive, C is not constant and instead varies with the loading rate. The strain rates in the material scale with the rate quantity $\dot{h}/h$ (e.g. Lucas and Oliver, 1999; Woodcock and Bahr, 2000) and thus C depends on material properties and $\dot{h}/h$. For a flow stress variation that follows Eq. (23), C can be approximated as

$$C = C_0 f(\dot{h}/h), \tag{24}$$

where C_0 is the quasi-static value of C, i.e. the value of C as $\dot{h}/h \to 0$. Therefore the function $f(\dot{h}/h)$ is positive with $f(0) = 1$. This suggests that if the motion of the indenter $h(t)$ were such that $\dot{h}/h$ were held constant, rate-dependent materials will follow Kick's law, with the constant C elevated above its quasi-static value.

We now apply these results to analyze the impact problem. In the following we will suppress the argument $\dot{h}/h$ and denote the function $f(\dot{h}/h)$ simply as f. During impact the velocity will decrease as the indenter advances into the material. The rate quantity $\dot{h}/h$ is not constant; it will decrease as indentation proceeds, eventually becoming equal to 0. During the loading phase the governing equation for the motion of the indenter is

$$m\ddot{h} + Ch^2 = m\ddot{h} + C_0 fh^2 = 0; \quad t \geqslant 0 \tag{25}$$

with initial conditions $h = 0$ and $\dot{h} = V_0$ at $t = 0$. If the values of m and V_0 are provided, and C_0 and f are known, Eq. (25) can be solved numerically to find the motion $h(t)$. As was done for the rate-independent case, Eq. (25) can be integrated to yield the instantaneous energy balance equation

$$\frac{1}{2}m\dot{h}^2 + \frac{1}{3}C_0 fh^3 - \frac{C_0}{3}\int_0^t (h^2\ddot{h} - h\dot{h}^2)f'\,\mathrm{d}t = \frac{1}{2}mV_0^2, \tag{26}$$

where f' represents the derivative of f with respect to its argument $\dot{h}/h$. Using the condition that at the peak indentation depth, $h = h_{\max}$, the velocity $\dot{h} = 0$ and $f(0) = 1$, the peak indentation depth can be determined to be:

$$h_{\max}^3 = \frac{3}{2}\frac{mV_0^2}{C_0} - \int_0^{t_1} (h\dot{h}^2 - h^2\ddot{h})f'\,\mathrm{d}t, \tag{27}$$

where t_1 is the time at which the peak depth is reached and $\dot{h} = 0$. Comparing with the rate-independent result, Eq. (4), it can be seen that for the rate-dependent case the peak depth is reduced.

To assess this analysis, finite element simulations were carried out in which the motion $h(t)$ was such that $\dot{h}/h$ was a constant whose value was varied over the range 2500–500,000 s^{-1}. The motion was of the form $h(t) = h_0 \exp(rt)$ where r is the value of $\dot{h}/h$. As the exponential curve does not satisfy $h(0) = 0$, a short period of constant velocity motion is imposed to connect the zero point with the exponential curve. The constant velocity takes place over a depth less than 2% of the total depth, so the influence of this region is expected to be small. Fig. 14(a) shows the form of the motion imposed for the case $r = 5000$ s^{-1}, while Fig. 14(b) shows a detail of the initial stages of the motion and the constant velocity segment that connects to the exponential curve.

Fig. 15 shows the load vs. depth curves for 1100 Al at various values of the rate parameter $\dot{h}/h$, along with the quasi-static result. It can be seen that in all cases the P–h curve is well represented by Kick's law, and from these results the constant C may be determined for each case. Good agreement with Kick's law
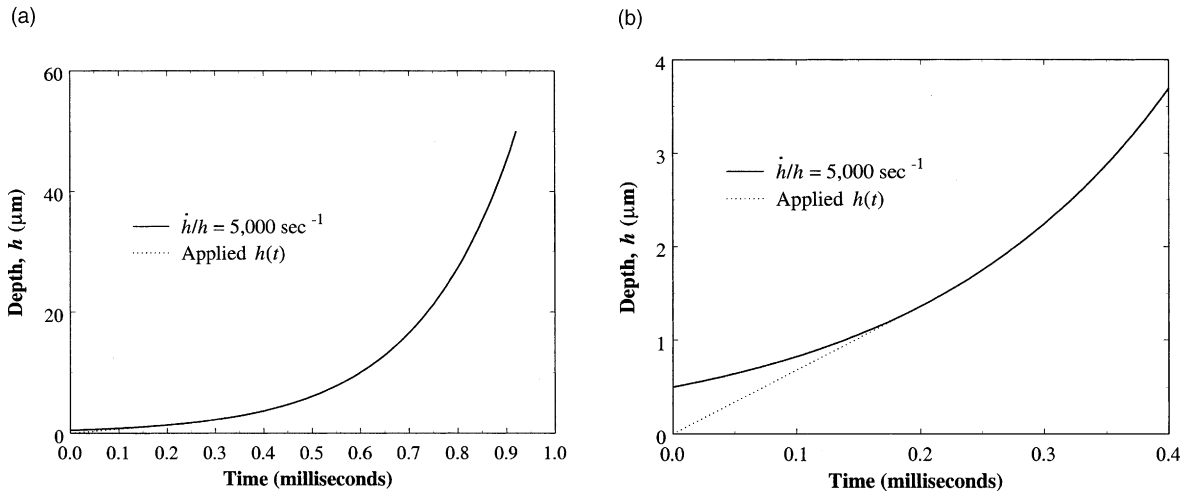
(a)

(b)

Fig. 14. (a) Applied $h(t)$ for rate-dependent indentation simulations. (b) Applied $h(t)$ showing constant velocity region.
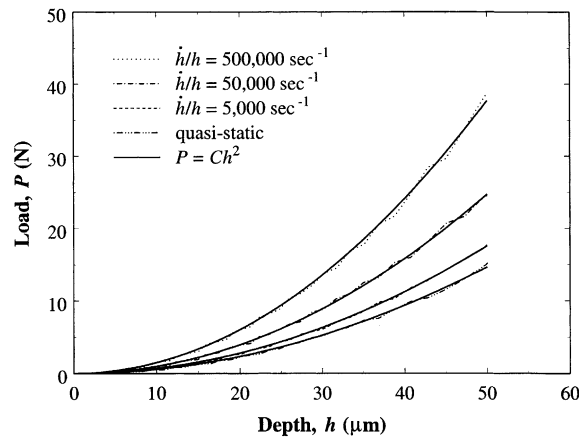

Fig. 15. Load vs. depth in dynamic indentation simulations at constant indentation loading rate $\dot{h}/h$ for 1100 Al, along with the quasi-static result.

was also found for 6061 Al. The variation of C as a function of $\dot{h}/h$ for the two different materials is plotted in Fig. 16. As expected, the strongly rate sensitive material shows greater sensitivity to the rate parameter $\dot{h}/h$. These results allow one to assess the form of $f(\dot{h}/h)$.

For the case where the strain rate influences the flow stress according to Eq. (23), we fit the variation of C as a function of $\dot{h}/h$ using the following function which involves two unknown parameters c and r_0

$$f(\dot{h}/h) \approx \left[1 + \left(\frac{\dot{h}/h}{r_0} \right)^c \right].$$
(28)

Within the range of parameters examined, we found that $c \approx b$ and $r_0 \approx 40\dot{\epsilon}_0 c$. Using the expression in Eq. (28) for $f(\dot{h}/h)$ the integral in Eq. (27) converges and was evaluated numerically for a range of impact velocities and masses using the values of $h(t)$, $\dot{h}(t)$ and $\ddot{h}(t)$ obtained from FEA. The peak depth was
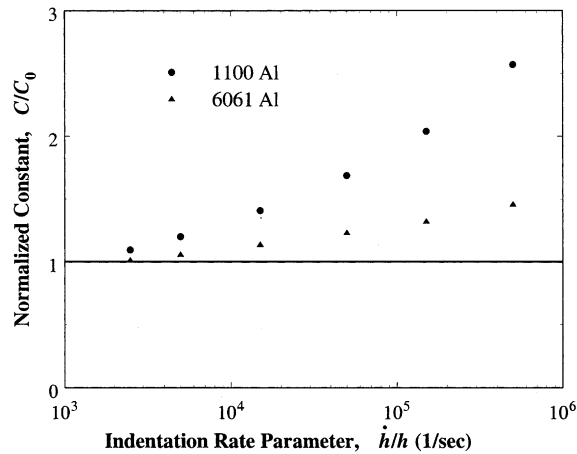
Fig. 16. Normalized constant C/C_0 vs. the indentation rate parameter $\dot{h}/h$.

predicted to within 5% in all cases examined, which implies that Eq. (24) is a valid representation of the variation of C under impact conditions. For the case of dynamic spherical indentation, Tirupataiah and Sundararajan (1991) define an average strain rate in the plastically deforming region, using expressions for the average strain and the contact time of the indenter. Koeppel and Subhash (1999) have suggested an average or effective strain rate equal to the velocity of the indenter divided by the final size of the indentation. The results presented here suggest an alternative approach in which the average variation in strain rate is followed during the impact through the function $f(\dot{h}/h)$. The present formulation suggests a way to obtain the dynamic material constants b and $\dot{\epsilon}_0$. The least information is either the displacement or velocity history for at least three dynamic indentation tests at different indenter kinetic energies $mV_0^2/2$. Equally well, one can use at least two dynamic indentation tests at different kinetic energies and one static test which provides C_0 directly.

5. Conclusions

An analysis of the impact of a sharp indenter has been presented. A solution describing the motion of the indenter has been given. The maximum depth of indentation, the residual depth of indentation, the time the indenter is in contact with the target and the rebound velocity have been provided.

The analytical results have been compared with dynamic rate-independent elastoplastic finite element simulations. The peak indentation depth, contact time and rebound velocity from the simulations were compared with the analytical predictions. The quantity $(C/\rho_{\text{target}})^{1/2}$ was found to be a characteristic velocity V_t for the dynamic sharp indentation problem and indicates the point at which the kinetic energy lost to the target becomes significant. It was found that the peak indentation depth and the contact time showed good agreement with the theoretical results up to impact velocities $\approx 0.1V_t$, while the rebound velocity deviated from the analytical prediction when the impact velocity exceeded $\approx 0.01V_t$. It appears that quantities associated with the loading phase (e.g. peak depth) show good agreement up to $\approx 0.1V_t$, while quantities associated with the rebound (e.g. rebound velocity) show good agreement only up to $\approx 0.01V_t$.

Rate-dependent plasticity has the effect of increasing the average contact pressure required for indentation, and increases the resistance to indentation. For the case of rate-dependent response in the impact problem the relationship between load and depth is no longer parabolic, and thus Kick's law is not valid

under these conditions. The problem can be solved by incorporating the relationship between the motion of the indenter and the dynamic flow properties of the material into the equation of motion for the indenter.

Acknowledgements

References

ASM, Source Book on Copper and Copper Alloys, 1979.

ASM, Atlas of Stress–Strain Curves, 1987.

Clifton, R.J., 2000. Response of materials under dynamic loading. Int. J. Solids Struct. 37, 105–113.

Frantz, R.A., Duffy, J., 1972. The dynamic stress–strain behavior in torsion of 1100-O aluminum subjected to a sharp increase in strain rate. J. Appl. Mech. 39, 939–945.

Giannakopoulos, A.E., Larsson, P.L., Vestergaard, R., 1994. Analysis of vickers indentation. Int. J. Solids Struct. 31, 2679–2708.

Giannakopoulos, A.E., Suresh, S., 1999. Determination of elastoplastic properties by instrumented sharp indentation. Scripta Mater. 40, 1191–1198.

Graham, G.A.C., 1973. Contribution to Hertz's theory of elastic impact. Int. J. Engng. Sci. 11, 409–413.

Huang, S., Clifton, R.J., 1985. Dynamic plastic response of OFHC Copper at high shear strain rates. In: Kawata, K., Shioiri, J. (Eds.), Macro and Micromechanics of High Velocity Deformation and Fracture, IUTAM, Tokyo, 63–73.

Klopp, R.W., 1984. Pressure-shear deformation of 4340 steel at strain rates of $10^5 \ s^{-1}$. In: M.Sc. Thesis. Brown University, Providence, RI.

Koeppel, G.J., Subhash, G., 1999. Characteristics of residual plastic zones under static and dynamic Vickers indentations. Wear 224, 56–67.

Lee, W.-S., Shyu, J.-C., Chiou, S.-T., 2000. Effect of strain rate on impact response and dislocation substructure of 6061-T6 aluminum alloy. Scripta Mater. 42, 51–56.

Li, C.H., 1982. A pressure-shear experiment for studying the dynamic plastic response of metals at shear strain rates of $10^5 \ s^{-1}$. In: Ph.D. Thesis. Brown University, Providence, RI.

Lucas, B.N., Oliver, W.C., 1999. Indentation power-law creep of high-purity indium. Metall. Mater. Trans. A 30, 601–610.

Marshall, D.B., Evans, A.G., Nisenholz, Z., 1983. Measurement of dynamic hardness by controlled sharp-projectile impact. J. Am. Cer. Soc 66, 580–585.

Nicholas, T., 1980. Tensile testing of materials at high rates of strain. Exp. Mech. 21, 177–185.

Senseny, P.E., Duffy, J., Hawley, R.H., 1978. Experiments on strain rate history and temperature effects during plastic deformation of close-packed metals. J. Appl. Mech. 45, 60–66.

Tirupataiah, Y., Sundararajan, G., 1991. A dynamic indentation technique for the characterization of the high-strain rate plastic flow behavior of ductile metals and alloys. J. Mech. Phys. Solids 39, 243–271.

Woodcock, C.L., Bahr, D.F., 2000. Plastic zone evolution around small scale indentations. Scripta Mater. 43, 783–788.